Available online at www.sciencedirect.com
SCIENCE DIRECT®
Physica A 336 (2004) 638–650
PHYSICA A
www.elsevier.com/locate/physa

Experiment and simulation of pedestrian counter flow

Motoshige Isobe, Taku Adachi, Takashi Nagatani*

Department of Mechanical Engineering, Shizuoka University, 432-8561 Hamamatsu, Japan

Received 12 January 2004

Abstract

Pedestrian counter flow is investigated by experiment and simulation. The experiment is performed for the channel with open boundaries. Two types of walkers, going to the right and to the left, are taken into account. The video recordings and measurements of individual arrival times are evaluated. The pattern formation and jamming transition are discussed. The experiment is mimicked by the lattice gas simulation where each person is simulated by a biased random walker taking into account following the front persons with the same direction. The experimental result is compared with the simulation result. It is shown that the arrival time obtained from experiment is consistent with that of the simulation. Also, the jamming transition does not occur in the experiment because of the finite size effect.

PACS: 05.70.Fh; 89.40.+k; 05.90.+m

Keywords: Pedestrian flow; Pattern formation; Evacuation dynamics; Phase transition

1. Introduction

Recently, traffic and pedestrian flows have attracted considerable attention [1–8]. Many observed self-organization phenomena in traffic and pedestrian flows have been successfully reproduced with physical methods. It has also encouraged physicists to study evacuation processes [9–15]. Pedestrian flow is a kind of many-body system of strongly interacting persons. The pedestrian flow dynamics is closely connected with the driven many particle system. To know the properties of pedestrian flow is important in our life. It is necessary to know the flow rate of pedestrian for rush hour and panic

* Corresponding author. Fax: +81-53-478-1048.
E-mail address: tmtnaga@ipc.shizuoka.ac.jp (T. Nagatani).

0378-4371/$ - see front matter
doi:10.1016/j.physa.2004.01.043

escape. It is also important to avoid the jammed state of pedestrians in the channel of the subway.

The typical pedestrian flows have been simulated by the use of a few models: the lattice-gas model of biased-random walkers [7–9], the molecular dynamic model of active walkers [6,13,14], and the mean-field rate-equation model [8]. Henderson has conjectured that pedestrian crowds behave similarly to gases or fluids [16]. Helbing has shown that human trail formation is interpreted as self-organization effect due to nonlinear interactions among persons [6]. The escape panic [11,13–15], counter channel flow [7], and bottleneck flow [9,19,20] have been studied numerically. Muramatsu et al. [17,18] have found that the jamming transition occurs in the pedestrian counter flow within a channel when the density is higher than the threshold [7]. Tajima et al. have shown that the clogging transition occurs in the unidirectional channel flow with a bottleneck if the density is higher than the threshold. The clogging transition is similar to that of the simple asymmetric exclusion model with a barrier.

It has been observed that the pedestrians file away in the subway. The filing of pedestrian is interesting from the points of view of the pattern formation. Does the filing enhance the flow rate? Does the jamming transition occur in the counter flow of pedestrian actually? How does the filing affect the jamming transition? Does the lattice gas simulation mimic the empirical pedestrian counter flow? Until now, little experiment has been known about the above questions. The works compared the simulation result with the experimental result is very scarce in the literature.

In this paper, we study the pedestrian counter flow experimentally and numerically. We would like to address the characteristic properties of the pedestrian counter flow. We carry out the experiment of pedestrian counter flow within the channel. The experiments are recorded by video cameras. The recordings are evaluated to derive the pedestrian flow properties. For comparison with the experiment, we present the lattice gas models to mimic the filing formation of pedestrian flow by extending the biased random walker model. We investigate the dependence of the arrival time on the density. We show that the filing and finite-size effect has the important effect on the pedestrian counter flow.

2. Experiment

We carry out the experiments for the pedestrian counter flow within the channel. Fig. 1 shows the schematic illustration of the experimental setup. The exact width of the channel is $W = 2$ m and its length $L = 12$ m. There are no obstacles in the channel. The left and right boundaries are open. The walkers are free to go out of the channel. Initially, there exist two types of walkers in the channel: the right walkers going to the right and the left walkers going to the left. Initially, the right walkers are positioned, randomly, within the left half of the channel. The left walkers are positioned, randomly, within the right half of the channel. A full circle indicates a right walker and the open circle indicates a left walker. Two video cameras are located at the left and right boundaries of the channel. The cameramen are able to observe all the walkers who exist within the channel by video cameras.

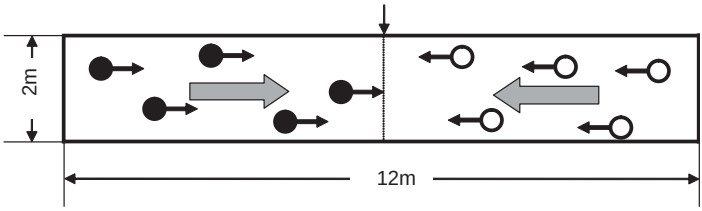

Fig. 1. Schematic illustration of the experimental setup. The exact width of the channel is $W = 2$ m and its length $L = 12$ m. There are no obstacles in the channel. The left and right boundaries are open. The walkers are free to go out of the channel. Initially, there are two types of walkers in the channel: the right walkers going to the right and the left walkers going to the left. Initially, the right walkers are positioned, randomly, within the left half of the channel. The left walkers are positioned, randomly, within the right half of the channel. A full circle indicates a right walker and the open circle indicates a left walker. When $t > 0$, all the walkers begin to move forward.

Correspondingly, at time $t = 0$, there are a constant number of walkers in the channel and each right (left) walker is standing at a random place within the left (right) half of the channel. All right (left) walkers move to seek for the right (left) boundary as soon as a cameraman shout a word of command. As soon as the right (left) walkers arrive at the right (left) boundary, they go through the boundary and leave the channel. The pedestrian counter flow process is then recorded by the two video cameras. We carry out the experiment, repeatedly, by varying the number of the walkers. Here, we set the experimental condition as such the case that the number of the right walkers equals that of the left walkers. Also, we asked the walkers to walk at normal speed.

By careful analysis of the video recordings, we determined the trajectory and arrival time of each walker. The individual arrival time was defined as the time elapsed between the shouting of the command and the moment when the respective walker arrived at the boundary at the end of the channel. Fig. 2 shows the time evolution of the experiment at $t = 0$, 5, 10, and 20 s for 60 walkers (corresponding to density 0.4). According as the walkers move forward, the right (left) walkers meet the left (right) walkers and the walkers file away. Accordingly, as the walkers avoid colliding with each other, the right (left) walkers follow the front right (left) walkers. The two types of walkers file alternately at $t = 10$ s. When the right (left) walkers go through a group of left (right) walkers, the filing of walkers disappears at $t = 20$ s. The arrival time of individual walker depends highly on the initial position.

We repeated the experiment 10 times under a constant number of walkers. The mean arrival time was obtained by averaging over all walkers and 10 experiments. Fig. 3(a) shows the plot of the mean arrival time against density. The density is calculated from the number of walkers as follows. The typical space occupied by a pedestrian in a dense crowd is about 0.4 m $\times$ 0.4 m. Thus, the occupied area of an individual is set as the value. Thus, 60 walkers correspond to density 0.4. The squares indicate the mean arrival time obtained from experiment. The full circles, open circles, and triangles indicate the arrival time obtained from the simulation explained in the following section. We carried out the experiment until the maximum number 70 of walkers. When the number of walkers is higher than 70, the walkers do not move forward, while the

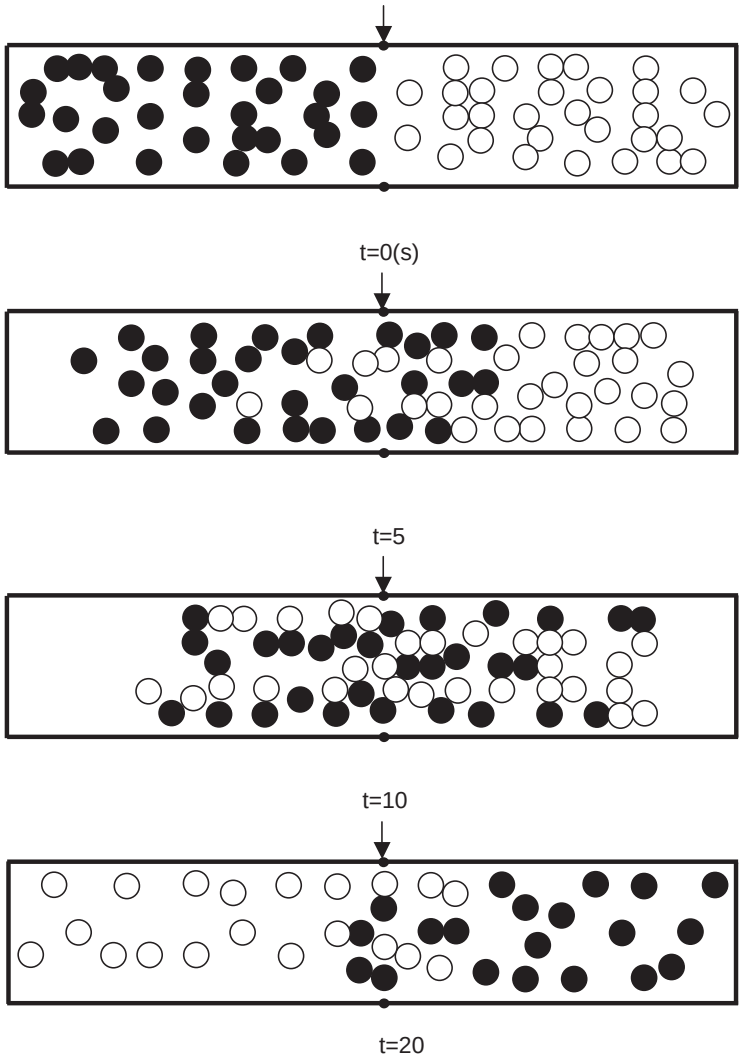

Fig. 2. Time evolution of the experiment at t=0, 5, 10, and 20 s for 60 walkers (corresponding to density 0.4). A full circle indicates a right walker and the open circle indicates a left walker.

channel is filled by about 150 walkers. The experiment with more walkers than 70 was very dangerous because the walkers fall over by pushing with each other.

We calculate the mean velocity of walkers from the experimental data. The velocity of the individual is defined as the length between the initial position and the boundary divided by the arrival time. The mean velocity is obtained by averaging over all walkers and 10 experiments. Fig. 3(b) shows the plot of the mean velocity against density. The squares indicate the mean velocity obtained from experiment. The full circles,

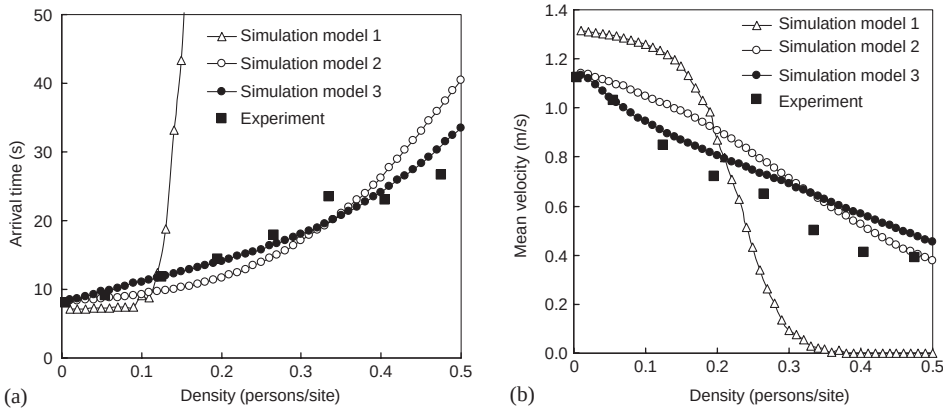

Fig. 3. (a) Plot of the mean arrival time against density. The squares indicate the experiment result. The triangles, open circles, and full circles indicate the simulation results for models 1, 2, and 3. (b) Plot of the mean velocity against density.

open circles, and triangles indicate the mean velocity obtained from the simulation explained in the following section.

3. Model and simulation

We extend the lattice gas models [7,21] to take into account the back step. We describe the extended lattice gas model for the pedestrian counter flow in a channel. The model is defined on the square lattice of $W \times L$ sites where W is the width of the channel and L is the length of the channel. The lattice gas model has two components of particles. One component particle represents the walker going to the right and the other component particle represents the walker going to the left. Each walker moves to the preferential direction. Each site contains only a single walker. The walker is inhibited from overlapping on the site. The excluded-volume effect is taken into account. When the walker arrives at the wall of channel, it is reflected by the wall and never goes out through the wall. The left and right boundaries are open. Each walker moves to the nearest neighbors according to the following configurations. Fig. 4 shows all the possible configurations of the right walker who is indicated by a full circle. The cross point indicates the site occupied by the other (right or left) walkers. Each walker hops to the unoccupied nearest neighbors. However, the transition (hopping) probability depends not only on the nearest neighbors but also on the other walkers existing in the front region where a walker watches forward. The front region of a walker is shown in Fig. 5. A walker determines his moving direction accordingly watching the front region shown in Fig. 5. The front region is divided into the three parts: left, central and right regions. The sites on the boundary between the left (right) and central regions overlap. Each region includes $M \times N$ sites. A walker wants to move into the region in which there are more other walkers with the same direction

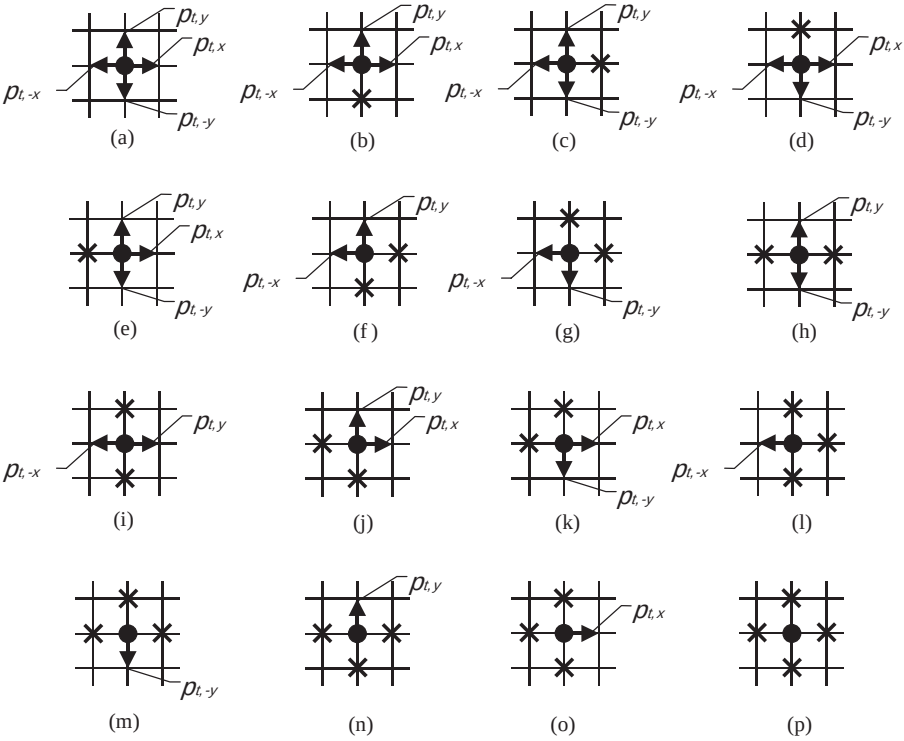

Fig. 4. All the possible configurations (a)–(p) of the right walker (going to the right) on the square lattice in model 3. The right walker is indicated by the full circle. The cross point indicates the site occupied by the other (right or left) walkers. Each walker can hop only to the unoccupied nearest neighbors.

than the other regions. The walker tends to follow the front walkers with the same direction.

The numbers of right walkers in the central, left, and right regions are defined as $n_{central}$, n_{left}, and n_{right}, respectively. The transition probabilities $p_{t,x}$, $p_{t,-x}\,p_{t,y}$, $p_{t,-y}$ of the right walker corresponding to each configuration are given by the following:

If $\max[n_{central}, n_{left}, n_{right}] = n_{central}$,

$$p_{t,x} = D_m + (1 - D_m)/4, \quad p_{t,-x} = p_{t,y} = p_{t,-y} = (1 - D_m)/4$$

for configuration (a),

$$p_{t,x} = D_m + (1 - D_m)/3, \quad p_{t,-x} = p_{t,y} = (1 - D_m)/3, \quad p_{t,-y} = 0$$

for configuration (b),

$$p_{t,x} = 0, \quad p_{t,-x} = p_{t,y} = p_{t,-y} = 1/3 \quad \text{for configuration (c)},$$

$$p_{t,x} = D_m + (1 - D_m)/3, \quad p_{t,-x} = p_{t,-y} = (1 - D_m)/3, \quad p_{t,y} = 0$$

for configuration (d),

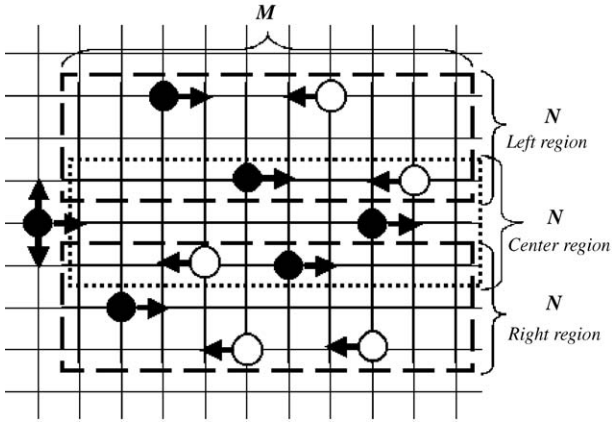

Fig. 5. The front region in which a walker watches to determine his moving direction. The front region is divided into the three parts: left, central and right regions. The sites on the boundary between the left (right) and central regions overlap. Each region includes $M \times N$ sites.

$$
\begin{aligned}
&p_{t,x} = D_m + (1 - D_m)/3, \quad p_{t,-x} = 0, \quad p_{t,-y} = p_{t,y} = (1 - D_m)/3 \\
&\quad \text{for configuration (e)}, \\
&p_{t,x} = p_{t,-y} = 0, \quad p_{t,-x} = p_{t,y} = 1/2 \quad \text{for configuration (f)}, \\
&p_{t,x} = p_{t,y} = 0, \quad p_{t,-x} = p_{t,-y} = 1/2 \quad \text{for configuration (g)}, \\
&p_{t,x} = p_{t,-x} = 0, \quad p_{t,y} = p_{t,-y} = 1/2 \quad \text{for configuration (h)}, \\
&p_{t,x} = D_m + (1 - D_m)/2, \quad p_{t,-x} = (1 - D_m)/2, \quad p_{t,y} = p_{t,-y} = 0 \\
&\quad \text{for configuration (i)}, \\
&p_{t,x} = D_m + (1 - D_m)/2, \quad p_{t,-x} = p_{t,-y} = 0, \quad p_{t,y} = (1 - D_m)/2 \\
&\quad \text{for configuration (j)}, \\
&p_{t,x} = D_m + (1 - D_m)/2, \quad p_{t,-x} = p_{t,y} = 0, \quad p_{t,-y} = (1 - D_m)/2 \\
&\quad \text{for configuration (k)}, \\
&p_{t,x} = p_{t,y} = p_{t,-y} = 0, \quad p_{t,-x} = 1 \quad \text{for configuration (l)}, \\
&p_{t,x} = p_{t,y} = p_{t,-x} = 0, \quad p_{t,-y} = 1 \quad \text{for configuration (m)}, \\
&p_{t,x} = p_{t,-x} = p_{t,-y} = 0, \quad p_{t,y} = 1 \quad \text{for configuration (n)}, \\
&p_{t,x} = 1, \quad p_{t,-x} = p_{t,y} = p_{t,-y} = 0 \quad \text{for configuration (o)}, \\
&p_{t,x} = p_{t,-x} = p_{t,y} = p_{t,-y} = 0, \quad \text{for configuration (p)}. \qquad (1)
\end{aligned}
$$

Here, D_m indicates the strength of the drift (bias): $D_m = D + n_{central}/(M \times N)$.

When $n_{central} = 0$, the strength of drift is consistent with that of the simple lattice gas model [7] with a back step (referred to as model 2). The original lattice gas model with no back step is referred to as model 1 [7]. The above model described by rule (1) is referred to as model 3. Model 3 is the extended one to take into account the back step in the lattice gas model proposed early by Tajima et al. [21].

If $\max[n_{central}, n_{left}, n_{right}] = n_{left}$,

$$
\begin{aligned}
&p_{t,x} = p_{t,-x} = p_{t,-y} = (1 - D_m)/4, \quad p_{t,y} = D_m + (1 - D_m)/4 \\
&\quad \text{for configuration (a)}, \\
&p_{t,x} = p_{t,-x} = (1 - D_m)/3, \quad p_{t,y} = D_m + (1 - D_m)/3, \quad p_{t,-y} = 0 \\
&\quad \text{for configuration (b)}, \\
&p_{t,x} = 0, \quad p_{t,-x} = p_{t,-y} = (1 - D_m)/3, \quad p_{t,y} = D_m + (1 - D_m)/3 \\
&\quad \text{for configuration (c)}, \\
&p_{t,x} = p_{t,-x} = p_{t,-y} = 1/3, \quad p_{t,y} = 0 \quad \text{for configuration (d)}, \\
&p_{t,x} = p_{t,-y} = (1 - D_m)/3, \quad p_{t,y} = D_m + (1 - D_m)/3, \quad p_{t,-x} = 0 \\
&\quad \text{for configuration (e)}, \\
&p_{t,x} = p_{t,-y} = 0, \quad p_{t,y} = D_m + (1 - D_m)/2, \quad p_{t,-x} = (1 - D_m)/2 \\
&\quad \text{for configuration (f)}, \\
&p_{t,x} = p_{t,y} = 0, \quad p_{t,-x} = p_{t,-y} = 1/2 \quad \text{for configuration (g)}, \\
&p_{t,x} = p_{t,-x} = 0, \quad p_{t,y} = D_m + (1 - D_m)/2, \quad p_{t,-y} = (1 - D_m)/2 \\
&\quad \text{for configuration (h)}, \\
&p_{t,x} = p_{t,-x} = 1/2, \quad p_{t,y} = p_{t,-y} = 0 \quad \text{for configuration (i)}, \\
&p_{t,x} = (1 - D_m)/2, \quad p_{t,-x} = p_{t,-y} = 0, \quad p_{t,y} = D_m + (1 - D_m)/2 \\
&\quad \text{for configuration (j)}, \\
&p_{t,x} = 1/2, \quad p_{t,-x} = p_{t,y} = 0, \quad p_{t,-y} = 1/2 \quad \text{for configuration (k)}, \\
&p_{t,x} = p_{t,y} = p_{t,-y} = 0, \quad p_{t,-x} = 1 \quad \text{for configuration (l)}, \\
&p_{t,x} = p_{t,y} = p_{t,-x} = 0, \quad p_{t,-y} = 1 \quad \text{for configuration (m)}, \\
&p_{t,x} = p_{t,-x} = p_{t,-y} = 0, \quad p_{t,y} = 1 \quad \text{for configuration (n)}, \\
&p_{t,x} = 1, \quad p_{t,-x} = p_{t,y} = p_{t,-y} = 0 \quad \text{for configuration (o)}, \\
&p_{t,x} = p_{t,-x} = p_{t,y} = p_{t,-y} = 0, \quad \text{for configuration (p)}. \qquad (2)
\end{aligned}
$$

Here, D_m indicates the strength of the drift (bias) and $D_m = D + n_{left}/(M \times N)$.

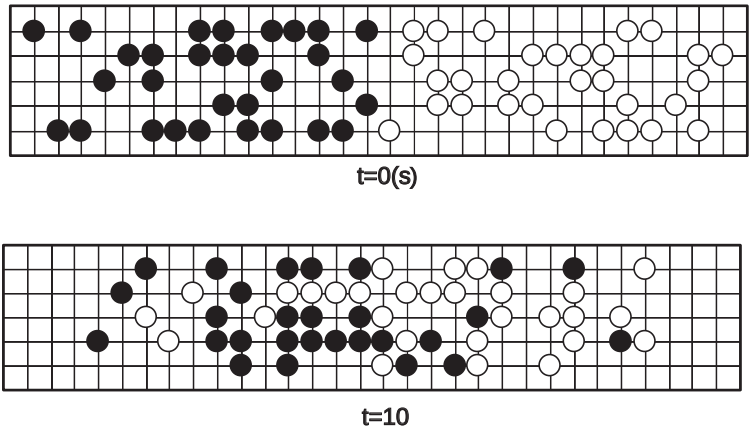

Fig. 6. Patterns obtained from simulation of model 3 at $t = 0$ and 10 s. According as the walkers move forward, the walkers file away.

If $\max[n_{central}, n_{left}, n_{right}] = n_{right}$, the transition probabilities are obtained by replacing y with $-y$ in Eq. (2). The drift is given by $D_m = D + n_{right}/(M \times N)$. When $D_m > 1$, we set $D_m = 1$. Similarly, the transition probabilities of the left walkers are obtained. Thus, the transition probability increases in the direction of the region where there exit more walkers with the same direction.

We carry out the computer simulation for models 1, 2, and 3. Initially, the right (left) walkers are distributed randomly on the left half (right half) within the channel. The number of the right walkers equals that of the left walkers. All the right (left) walkers are numbered randomly from 1 to $N_{particle}$ where $N_{particle}$ is the number of right (left) walkers existing within the channel. At $t = 0$, all the walkers are at rest. When $t > 0$, all the walkers begin to move. Following the above rule, all the numbered right walkers are in order updated. After updating all the right walkers, all the numbered left walkers are in order updated. After all the walkers are updated, if the walkers arrive at the boundaries, their walkers are removed from the channel. After the above procedure is carried out, one time step is completed. The above procedure is repeated.

For mimicking the experimental counter flow, we choose the lattice spacing as 0.4 m, since the typical space occupied by a pedestrian in a dense crowd is about 0.4 m×0.4 m. We therefore use $L = 30$ and $W = 5$ for the channel on the square lattice. Furthermore, we choose the unit time as 0.25 s and the drift D as 0.7. Then, the forward moving speed is 1.24 m/s if there are no other walkers. The speed is comparable with the speed 1.1–1.3 m/s obtained from the experiment. Also, we set the front watching region $M = 3$ and $N = 10$.

We present the simulation result obtained by the above. Fig. 6 shows the patterns obtained from model 3 at $t = 0$ and 10 s. According as the walkers move forward, the walkers file away. The two kinds of filings appear: the one is the filing of right walkers and the other is the filing of left walkers. When the filing of right walkers meets that of left walkers, they avoid colliding with the other.

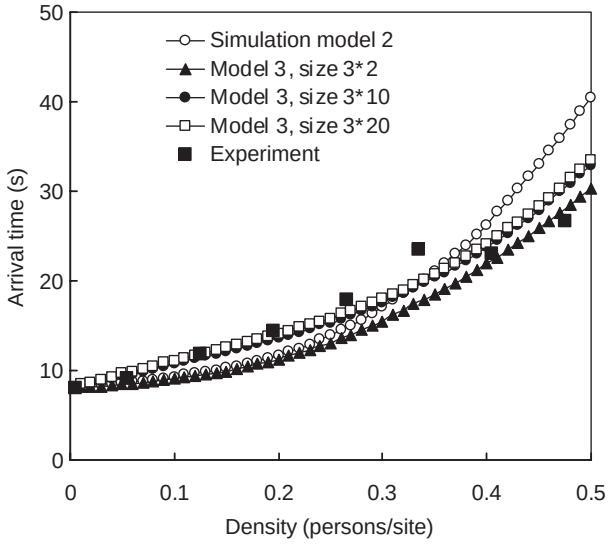

Fig. 7. Effect of the front watching area $M \times N$ on the arrival time in model 3. Plots of the arrival time against density for $N = 2$, 10, and 30 where $M = 3$ and the values of other parameters are the same as those in Fig. 3(a).

Fig. 3(a) shows the plot of the mean arrival time against density. The arrival time is defined as such time that a walker arrives at the boundary. The mean value is obtained by averaging over all the walkers and 1000 simulations. The squares indicate the mean arrival time obtained from experiment. The triangles, open circles, and full circles indicate the arrival time obtained from the simulation results for models 1, 2, and 3. The simulation result of model 3 is consistent with the experimental result.

We calculate the mean velocity of walkers from the simulation. The mean velocity of the walkers is defined as the number of the forward moving walkers divided by the total number of walkers. The mean velocity is obtained by averaging over 1000 simulations. Fig. 3(b) shows the plot of the mean velocity against density. The squares indicate the mean velocity obtained from experiment. The triangles, open circles, and full circles indicate the mean velocity obtained from the simulations 1, 2, and 3.

We study the effect of the front watching area $M \times N$ on the arrival time in model 3. Fig. 7 shows the plots of the arrival time against density for $N = 2$, 10, and 30 where $M = 3$ and the values of other parameters are the same as those in Fig. 3(a). With increasing N, the filing becomes more and more clear. The mean arrival time increases a little bit. The open circles indicate the simulation result for model 2. The full squares indicate the experimental result. The simulation result for $N = 10$ agrees well with the experimental result.

We study the effect of the channel width W and length L on the mean arrival time. Fig. 8 shows the plots of the mean arrival time against density for $W = 5$, 10, 20, and 50 where $L = 30$. With increasing W, the arrival time increases and approaches to

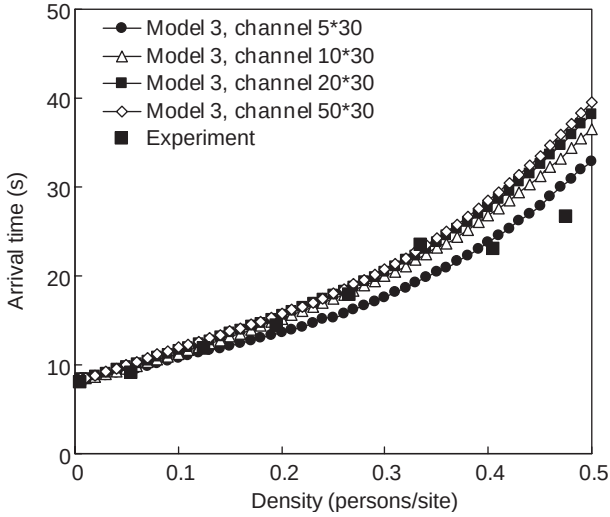

Fig. 8. Plots of the mean arrival time against density for $W = 5$, 10, 20, and 50 where $L = 30$.

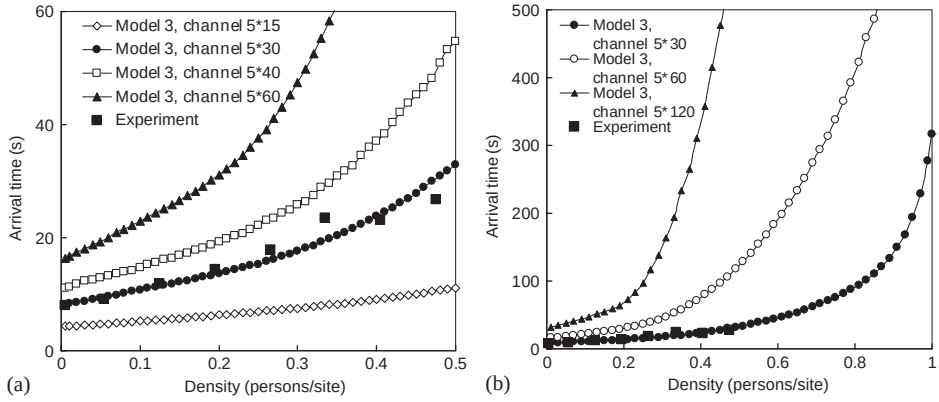

Fig. 9. (a) Plots of the mean arrival time against density for $L = 15$, 30, 40, and 60 where $W = 5$. (b) Plots of the mean arrival time against density until full density for $L = 30$, 60, and 120.

the limiting values. Fig. 9(a) shows the plots of the mean arrival time against density for $L = 15$, 30, 40, and 60 where $W = 5$. The mean arrival time increases highly accordingly the length L increases. Fig. 9(b) shows the plots of the mean arrival time against density until full density for $L = 30$, 60, and 120 where $W = 5$. For the short length L, the jamming transition does not occur but appears for an infinite length. In our experiment, the jamming transition did not occur between freely moving phase and perfectly jammed phase in which walkers cannot move. This is due to the finite size effect.

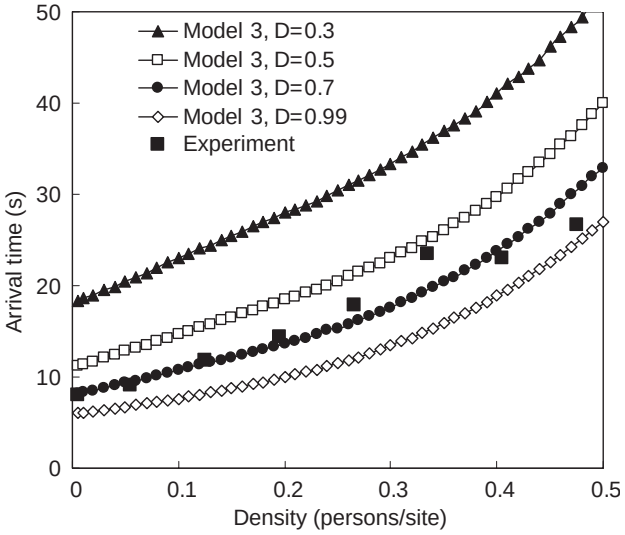

Fig. 10. Plot of the mean arrival time against density for $D = 0.3$, 0.5, 0.7, and 0.99 in model 3 where $W = 5$, $L = 30$, $M = 10$, and $N = 3$.

We study the dependence of the mean arrival time on the drift D. Fig. 10 shows the plot of the mean arrival time against density for $D = 0.3$, 0.5, 0.7, and 0.99 in model 3 where $W = 5$, $L = 30$, $M = 10$, and $N = 3$. The mean arrival time increases highly with increasing drift D. The experimental result (full square point) is consistent with the simulation result $D = 0.70$. Thus, the extended lattice gas model 3 reproduces the experimental result well. However, models 1 and 2 do not mimic the experimental counter flow quantitatively but explain the empirical pedestrian behavior qualitatively.

4. Summary

We have investigated the pedestrian counter flow in the channel by experiment and simulation. We have clarified the characteristic properties of pedestrian channel flow. We have discussed the pattern formation, pedestrian speed, and jamming transition. We have shown that the simulation model taking into account the front watching effect and back step is able to mimic, quantitatively, the pedestrian behavior observed experimentally in the counter flow. We have compared the simulation result obtained by some models with the experimental result. We have shown that the jamming transition does not occur in the experiment because of the finite size effect.

This study is the first that the experiment was compared with the simulation in the pedestrian counter flow. This study will be useful to estimate the pedestrian flow characteristics in the subway or at rush hour.

References

[1] T. Nagatani, Rep. Prog. Phys. 65 (2002) 1331.
[2] D. Helbing, Rev. Mod. Phys. 73 (2001) 1067.
[3] D. Chowdhury, L. Santen, A. Schadschneider, Phys. Rep. 329 (2000) 199.
[4] B.S. Kerner, Phys. World 12 (1999) 25.
[5] D.E. Wolf, M. Schrekenberg, A. Bachem (Eds.), Traffic and Granular Flow, World Scientific, Singapore, 1996.
[6] D. Helbing, P. Mulnar, Phys. Rev. E 51 (1995) 4282.
[7] M. Muramatsu, T. Irie, T. Nagatani, Physica A 267 (1999) 487.
[8] T. Nagatani, Physica A 300 (2001) 558.
[9] Y. Tajima, T. Nagatani, Physica A 292 (2001) 545.
[10] C. Burstedde, K. Klauck, A. Schadschneider, J. Zittartz, Physica A 295 (2001) 507.
[11] A. Kirchner, A. Schadschneider, Physica A 312 (2002) 260.
[12] H. Klupfel, M. Meyer-Konig, J. Wahle, M. Schreckenberg, in: S. Babdini, T. Worsch (Eds.), Proceedings of the Fourth International Conference, CA, Springer, London, 2000, p. 63.
[13] D. Helbing, I. Farkas, T. Vicsek, Nature 407 (2000) 487.
[14] D. Helbing, I. Farkas, T. Vicsek, Phys. Rev. Lett. 84 (2000) 1240.
[15] D. Helbing, M. Isobe, T. Nagatani, K. Takimoto, Phys. Rev. E 67 (2003) 067101.
[16] L.F. Henderson, Nature 229 (1971) 381.
[17] M. Muramatsu, T. Nagatani, Physica A 275 (2000) 281.
[18] M. Muramatsu, T. Nagatani, Physica A 286 (2000) 377.
[19] Y. Tajima, K. Takimoto, T. Nagatani, Physica A 294 (2001) 257.
[20] T. Itoh, T. Nagatani, Physica A 313 (2002) 695.
[21] Y. Tajima, K. Takimoto, T. Nagatani, Physica A 313 (2001) 709.